Available online at www.sciencedirect.com
ScienceDirect
Journal of the Mechanics and Physics of Solids
55 (2007) 1439–1461

JOURNAL OF THE MECHANICS AND PHYSICS OF SOLIDS

www.elsevier.com/locate/jmps

On criteria for dynamic adiabatic shear band propagation

Sergey N. Medyanik[a,1], Wing Kam Liu[a,*], Shaofan Li[b]

[a]*Department of Mechanical Engineering, Northwestern University, 2145 Sheridan Road, Evanston, IL 60208, USA*
[b]*Department of Civil and Environmental Engineering, University of California, Berkeley, CA 94720, USA*

Received 4 December 2005; received in revised form 20 December 2006; accepted 26 December 2006

Abstract

In this work, we postulate the physical criterion for dynamic shear band propagation, and based on this assumption, we implement a numerical algorithm and a computation criterion to simulate initiation and propagation of dynamic adiabatic shear bands (ASBs). The physical criterion is based on the hypothesis that material inside the shear band region undergoes a dynamic recrystallization process during deformation under high temperature and high strain-rate conditions. In addition to providing a new perspective to the physics of the adiabatic shearbanding process and identifying material properties that play a crucial role in defining the material's susceptibility to ASBs, the proposed criterion is instrumental in numerical simulations of the propagation of ASBs when multi-physics models are adopted to describe and predict the complex constitutive behavior of ASBs in ductile materials. Systematic and large scale meshfree simulations have been conducted to test and validate the proposed criterion by examining the formation, propagation, and post-bifurcation behaviors of ASBs in two materials, 4340 steel and OFHC copper. The effects of heat conduction, in particular the length scale introduced by heat conduction, are also studied. The results of the numerical simulations are compared with experimental observations and a close agreement is found for various characteristic features of ASBs, such as the shear band width, speed of propagation, and maximum temperature.

Keywords: Strain localization; Adiabatic shear band propagation; Meshless methods; Dynamic recrystallization; Failure criterion

*Corresponding author. Tel.: +1 847 491 7094; fax: +1 847 491 3915.
E-mail addresses: medyanik@wsu.edu (S.N. Medyanik), w-liu@northwestern.edu (W.K. Liu).
[1]Current address: Washington State University, School of Mechanical and Materials Engineering, Pullman, WA,USA.

0022-5096/$ - see front matter © 2007 Elsevier Ltd. All rights reserved.
doi:10.1016/j.jmps.2006.12.006

1. Introduction

Shear bands are relatively narrow regions of highly localized shear deformation. The shear banding phenomenon occurs under different loading conditions in various materials (e.g., metals and alloys, plastics, geotechnical materials, such as rocks and soils, and granular materials). When metals and alloys deform under high strain rate loading, a special type of shear band is often formed known as the *adiabatic shear band* (ASB), which has a width of the order of several microns to several hundreds of microns. Here, the adjective *adiabatic* refers to the unique feature of the ASB that during an extensive plastic deformation a large amount of heat is generated inside the shear band, and since the temporal scale of the shear deformation is much shorter than that of heat conduction, most of the generated heat stays inside the shear band. However, this does not mean that heat diffusion is not important for the shear banding processes. In fact, due to the extremely large temperature gradients across the shear band areas, heat diffusion plays a crucial role in the process. Nevertheless, the term "adiabatic shear band" is generally used to denote the shear localization in metals and alloys under high strain and strain rate conditions (see, e.g., Wright, 2002), and we are going to follow this notation in the current work.

Adiabatic shear banding in metals and alloys has been extensively studied for several decades. For detailed background information, readers may consult the two major monographs on this subject: Bai and Dodd (1992) and Wright (2002) and literature therein. The former provides excellent descriptions and discussions on physics and experiments of ASBs, while the latter focuses on mathematical and mechanical modeling of ASBs. A concise review of the subject can be also found in a book by Meyers (1994).

The propagation of ASBs is a major ductile failure mechanism when ductile materials are subjected to impact, penetration, and explosive loads. It not only triggers both mode-I and mode-II fractures but also results in a virtual fracture, or material separation damage, along the path of a shear band propagation. This phenomenon more or less resembles the mode-II crack propagation in solids. However, the ASB propagation is far less studied and understood because this is a more complex physical phenomenon than the crack propagation. There is virtually no analytical benchmark solution for the ASB propagation in multi-dimensions. So far, the most efficient way to study the ASB propagation is through numerical simulations.

One school of study on ASB propagation is to derive analytical solution of ASB propagation as a singular plastic surface extension (strain localization is a weak discontinuity over a surface). This is different from singular plastic wave front propagation, because ASB propagates perpendicular to the normal of the singular surface, whereas the weak singular wave propagation is along the normal to the singular surface. There are a handful of analytical ASB solutions available that account for heat conduction. However, for a tractable solution, most of these studies neglect dynamic effects, use simplified constitutive relations as well as adopt asymptotic analysis or approximations in the solution procedure (e.g., Wright, 1990). In addition, most of these ASB solutions are about ASB formation rather than ASB propagation. Moreover, most of these solutions are obtained for the 1D case, while multi-dimensional ASB solutions are scarce (see, e.g., Wright, 2002). In fact, analytical studies of the ASB problem face serious difficulties, even in the simplest case of mode-III loading (Zhang and Clifton, 2003); too

many simplifications and assumptions have to be made, and a general theory on ASB propagation is still lacking.

Another school of study of ASB propagation is to model it by simulating the actual ASB propagation via numerical computations and constitutive modeling. This has been done by using finite element methods (e.g., Zhou et al., 1996b; Bonnet-Lebouvier et al., 2002) as well as meshfree methods (e.g., Li et al., 2001, 2002). More recently, Areias and Belytschko (2006) have modeled shear band propagation using the extended finite element method (XFEM).

One of the major issues or difficulties in the simulation of ASB propagation is the onset criterion for ASB growth and propagation. Unlike crack propagation, the criterion for the ASB propagation is still an open subject. Currently, the most successful dynamic ASB simulations are using multi-physics modeling, i.e., different constitutive relations are used for the material inside and outside the ASB to take into account the phase-transformation undergoing inside the ASB (e.g., Zhou et al., 1996b; Li et al., 2002). The advantages of the multi-physics modeling are two fold: (1) it provides a convenient way to simulate physical phenomenon with different length and time scales, and (2) the criterion of ASB propagation becomes the criterion for switching from one set of constitutive equations to another, which simplifies the numerical computations.

However, the key to a successful dynamic ASB simulation is the criterion for the onset of the ASB growth and propagation. To the authors' knowledge, there is no universally accepted criterion for the initiation and propagation of dynamic ASB. The key issue here is what is the actual physical process controlling the ASB propagation. The subject is not well understood in both its physical origin as well as its simulation.

In this work, we venture to propose a new physical criterion for the ASB propagation, and we will use this criterion in the modeling of the initiation and propagation of dynamic ASBs as an indirect way to validate the postulate, or hypothesis, itself.

We postulate that the ASB formation and propagation is directly related to and may be dictated by the dynamic recrystallization inside the ASB. The undergoing dynamic recrystallization (DRX) process inside an ASB is the very process of microstructure reformation and evolution inside the ASB. Therefore, the formation and propagation of the ASB can be described by the onset conditions as well as the parameters of the DRX inside the ASB.

The new criterion of the ASB propagation is modeled by the onset condition of DRX in terms of critical temperature of DRX. We postulate that when temperature at a material point reaches a recrystallization temperature, which is a function of strain rate, instant softening will occur at that point, leading to an instant stress collapse—a ductile failure.

The main idea of our work is that for most ductile materials under high strain rate loading conditions there are two major factors which contribute to the material's susceptibility to adiabatic shear banding: (1) DRX properties, and (2) thermal properties (thermal conductivity), which, to the best of the authors' knowledge, is novel.

The paper is organized as follows. In Section 2, a new ductile failure criterion is introduced and justified based on the physics of adiabatic shearbanding. In Section 3, we briefly outline the numerical method, governing equations, and discuss the constitutive models used in the simulations. Finally, results of the numerical simulations based on the new criterion are presented in Section 4.

2. Dynamics ductile failure criterion

2.1. Why we need a ductile failure criterion

According to experimental data (e.g., Marchand and Duffy, 1988), onset of the ductile failure via shearbanding occurs in a sudden, drastic way. The same studies show that immediately following the onset of the ductile failure, the stress at the material point drops almost vertically to about a quarter of its peak value. We call this sudden drop, a ductile failure, or a stress collapse, and attempt to derive a criterion that can predict the onset of such a state.

It appears to be rather difficult, if not impossible at all, to represent a complex material behavior at all stages of the deformation process, including the shear band formation and development, by a single constitutive law that has a functional form not changing throughout the whole deformation process. Today, the most successful numerical simulations of ASB propagation (e.g., Zhou et al., 1996b; Li et al., 2001, 2002) were obtained using multi-physics models. In these models, two different constitutive laws were used, one for the material inside the shear band region, which is often referred to as a *damage* model, and the other for the surrounding matrix material. We believe that the complexity of dynamic ASB propagation can be best captured in multi-physics approach, when different constitutive laws are employed, each being better suitable for the material modeling at a particular stage of the deformation process. In this case, a failure criterion is needed to determine the moment when the switch between the different constitutive models has to be done.

An excellent discussion on the necessity of a ductile failure criterion was recently given by Schoenfeld and Wright (2003), who identified the need for the introduction of what they call a "shear damage" in order to model the stress collapse state inside an ASB, as well as the need for a ductile failure criterion in order to determine the right timing at which it should occur. Such a criterion, if properly designed, could also shed some light on the physics of adiabatic shearbanding, as well as help to predict the susceptibility of different materials to this type of failure. It seems that at this point the ductile failure criterion is very much needed by the engineering community, where it could find vast applications in different areas of engineering analysis and design.

2.2. Overview of the existing criteria

Before discussing the recrystallization hypothesis, we first review the main ASB propagation criteria currently used for the ASB modeling. A number of such criteria have been proposed in the literature in order to model the stress collapse state inside the ASBs. Most of these criteria are either ad hoc or empirical in nature.

Batra and co-workers have used two types of failure criteria: one based on strain and the other based on stress (see, e.g., Batra and Lear, 2004). In the first case, ductile failure occurs when the equivalent plastic strain at a material point reaches critical value $\bar{\varepsilon}_{cr}$, which is a constant. The applied values of $\bar{\varepsilon}_{cr}$ were 0.5 and 1.0. In the second case, the ductile failure is set to occur when, in a process of material softening, the equivalent plastic stress (or the maximum shear stress) at a material point drops to the value equal to 0.8 (in other simulations 0.9) of its peak value. For instance, Batra and Kim (1992) used the following criterion:

$$\sigma_{max} = 0.8\sigma_{peak} \quad \text{and} \quad \dot{\bar{\varepsilon}}^{p}_{e} > 0, \tag{1}$$

where $\sigma_{\max}$ and σ_{peak} are correspondingly the current maximum shear stress and the peak shear stress value ever reached at that point, $\dot{\varepsilon}_e^p$ is the effective plastic strain rate, and the condition $\dot{\varepsilon}_e^p > 0$ is necessary to ensure that the shear stress drop is due to material softening, not elastic unloading.

The most elaborate ductile failure criterion so far is based on strain and was introduced by Zhou et al. (1996b), who suggested that the critical strain is dependent on the strain rate:

$$\bar{\varepsilon}_{\text{cr}} = \varepsilon_1 + (\varepsilon_2 - \varepsilon_1)\frac{\dot{\varepsilon}_r}{\dot{\varepsilon}_r + \dot{\bar{\varepsilon}}}, \tag{2}$$

where ε_1, ε_2, $\dot{\varepsilon}_r$ are empirical parameters and $\varepsilon_1 < \varepsilon_2$. This form of failure criterion suggests that the critical strain reduces with the growth of strain rate, being equal to ε_2 when the strain rate is zero and approaching ε_1 as the strain rate grows to infinity.

The form (2) of the failure criterion has been based on the experimental observations that for higher strain rates the localization of deformation occurs at smaller strains. Failure criterion (2) was successfully used in the recent simulations of the dynamic shear band propagation by Li et al. (2001, 2002). The values of the parameters used with this criterion by Zhou et al. (1996b) and Li et al. (2001, 2002) were: $\varepsilon_1 = 0.04$, $\varepsilon_2 = 0.3$ and $\dot{\varepsilon}_r = 4 \times 10^4\,\text{s}^{-1}$. However, the physical meaning of the critical strain is rather ambiguous, as is the meaning of the parameters entering the criterion formulation. Realizing its shortcomings, Zhou et al. (1998) tried to propose a criterion based on J-integral, similar to that used in the crack propagation analysis. This generalized path-independent J-integral for dynamic conditions is given by

$$J = \int_\Gamma \left[\left(\int_0^t \boldsymbol{\tau} : \mathbf{D}\,\mathrm{d}t - \int_{T_0}^T \boldsymbol{\tau} : \mathbf{I}\,\mathrm{d}T + \frac{1}{2}\rho\dot{\mathbf{u}}\cdot\dot{\mathbf{u}} \right) \mathrm{d}x_2 - \mathbf{t}\cdot\frac{\partial \mathbf{u}}{\partial x_1}\,\mathrm{d}s \right] + \int_A \left[\alpha(\boldsymbol{\tau} : \mathbf{I})\frac{\partial T}{\partial x_1} + \rho\dot{\mathbf{u}}\cdot\frac{\partial \mathbf{u}}{\partial x_1} - \rho\dot{\mathbf{u}}\cdot\frac{\partial \dot{\mathbf{u}}}{\partial x_1} \right] \mathrm{d}A. \tag{3}$$

Here, Γ is an arbitrary contour surrounding the crack tip, A is the area bounded by Γ, x_1 and x_2 are coordinates in the reference configuration, $\mathbf{u}$ is the displacement, $\boldsymbol{\tau}$ is a Kirchhoff stress tensor, $\mathbf{D}$ is the rate of deformation tensor, $\mathbf{t}$ is the traction on the contour, t is the time, and T is the temperature.

In their analysis, Zhou et al. use a series of contours of different sizes surrounding the tip of the prenotch, where the ASB is expected to initiate. For each of these contours, the value of the J-integral remains the same until the propagating ASB reaches the contour, which corresponds to the moment, when a failure criterion is satisfied at that material point on the contour. However, the J-integral based criterion was never fully implemented or justified.

There were also efforts to develop a failure criterion based on the mathematical analysis of the shearbanding problem. For instance, Schoenfeld and Wright (2003) have used a simple 1D shear problem formulation and the previously derived scaling laws to obtain such a criterion. This analysis required assumptions and simplifications, and, as a result, the derived criterion was somewhat obscure and its applicability to multiple dimensions was not clear. Furthermore, it seems that any criterion based on the material instability argument and using a single constitutive law has an inherent flaw: it may only give a criterion for the shear band *formation*, and not that for the shear band *propagation*.

We believe that it is imperative to discriminate between the two physical phenomena: the shear band formation and shear band propagation. The shear band *formation* is a relatively slow process of the localization of deformation, which is related to the phenomenon of material instability. Whereas the shear band *propagation* is a fast dynamic process of the evolution of the phase transition region. The ASB propagation is characterized by the relatively well defined shear band tip area and a growing damaged (shearbanded) "second phase" region. We believe that the former phenomenon (ASB formation) may be modeled using a single constitutive law and the material instability criterion, while the latter one (ASB propagation) should be considered as a moving boundary problem of a multi-phase transition, which has to be modeled using a multi-physics constitutive modeling approach.

2.3. Motivation for a new type of criterion

The existing ductile failure criteria for ASB propagation have some shortcomings, which have hindered accurate predictive simulations. Many important characteristic features of the dynamic ASBs, such as the shear band width, speed of propagation, temperature rise inside an ASB, as well as the temperature at which the shear band initiates, have rarely been reproduced, and have never been reproduced altogether in one numerical simulation.

One of the major shortcomings of the current shear band modeling techniques is severe mesh-dependency of the resulting shear band width. All the failure criteria that are based on strain or stress are intrinsically mesh dependent as the strain and stress tend to localize in the narrowest possible band (usually the size of a background mesh cell) when no additional regularization to the problem is introduced. Fig. 1 demonstrates a fully developed ASB modeled using criterion (2) and two different meshes, the right one being twice as fine as the left. Here, most of shear deformation is localized in one background mesh cell revealing a severe mesh-dependency of the obtained shear band width, while the areas next to the shear band seem to be almost non-deformed. Such a result is very typical for shear band modeling and in this case was obtained even in the presence of heat conduction. The presented picture of a microstructure of an ASB and the surrounding

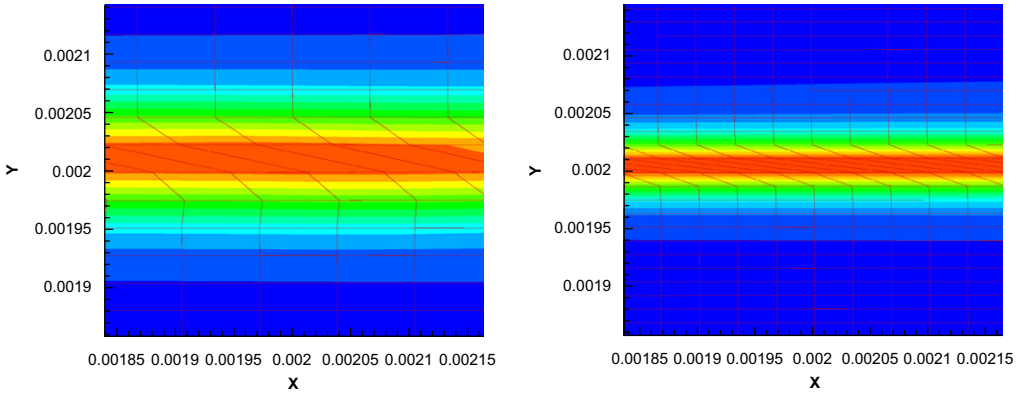

Fig. 1. Adiabatic shear band obtained using a strain-based stress collapse criterion. Severe mesh-dependency of the shear band width is observed.

areas does not look realistic when compared to experimental results where shear bands always have finite width and a transition between the shear localized and homogeneously deformed domains is usually more smooth.

Furthermore, since the parameters of the currently existing ductile failure criteria are not related to the actual material properties or real physics behind the shearbanding deformation processes, they usually have to be selected by matching *already known* experimental data and very often cannot be extrapolated to the more general cases. Therefore, they can be only used to simulate a very limited range of problems that they were fitted for. This prevents such simulations from making objective *predictions* of the material behavior.

To build a predictive model, we are seeking a new type of ductile failure criterion, which would be more universal and provide physically sound simulations capturing various ASB features. In addition, the new criterion should be based on the actual material properties and reflect the deformation mechanisms behind the adiabatic shearbanding.

2.4. DRX and ASBs

The new ductile failure criterion that we are proposing is based on a physical phenomenon called *dynamic recrystallization.* DRX is a phase-transformation process that takes place in many ductile materials when they deform at high temperatures, high strains, and high strain rates. This phenomenon causes a dramatic change in the material's microstructure, considerably refining the microscopic grain size, and is accompanied by a sudden reduction of the dislocation density, finally leading to an instant softening.

Many experimental results (e.g., Meyers and Pak, 1986; Andrade et al., 1994; Mescheryakov and Atroshenko, 1995; Hines and Vecchio, 1997; Xu et al., 2001; Meyers et al., 2001) have shown that recrystallization takes place inside the ASBs for a large number of metals and alloys. For instance, it was found (Meyers and Pak, 1986; Hines and Vecchio, 1997) that the microstructure within the shear band consists of fine recrystallized grains, with the finer grains located closer to the center of the band. Meyers and Pak (1986) were the first to observe the recrystallized grains and propose DRX as a possible mechanism of deformation inside an ASB.

It was also shown that recrystallization occurs *during* (not after) the deformation process, which proves that the recrystallization is *dynamic* (not static) and happens simultaneously with the ASB propagation. McQueen and Bergerson (1972) have investigated the differences between static and dynamic types of recrystallization and provided criteria on how to distinguish between them. According to their observations, the size of the recrystallized grains is smaller in the case of DRX. In addition, statically recrystallized material usually contains a lot of annealing twins, which usually form during cooling that follows the deformation, while in case of DRX the number of annealing twins is very low. Following these guidelines, Hines and Vecchio (1997) have analyzed the microstructure of ASBs in copper, and they found very small refined grains inside the ASBs along with a low evidence of annealing twins. They have also examined several possible mechanisms of static recrystallization and concluded that diffusion-based mechanisms of static recrystallization were kinetically too slow (by at least several orders of magnitude) to cope with the speed of deformation inside an ASB. Based on this evidence, static recrystallization was effectively ruled out, and DRX during adiabatic shearbanding was confirmed.

Several models explaining mechanisms of DRX occurring during adiabatic shearbanding have been proposed. Meyers and Pak (1986) proposed a simple mechanism for plastic deformation during ASB propagation that involves micrograin rotation and sliding of micrograin boundaries. Another mechanism for DRX inside ASBs is based on the formation of elongated dislocation cells (e.g., Nesterenko et al., 1997) that later break up into smaller subgrains. Hines et al. (1998) proposed a mechanical subgrain rotation model to account for the recrystallized grains inside the ASBs. In that model, initially large single-crystal grains are divided into several elongated subgrains. Then these elongated subgrains break into much smaller equiaxed ones that rotate in order to accommodate high deformation rates. In general, these models are quite similar and usually involve some mechanical means, such as micrograin sliding and rotation, in order to allow for very high strain rates that occur during adiabatic shearbanding and are difficult to explain by conventional deformation mechanisms.

Based on the experimental evidence as well as analyses in the literature, the DRX has been confirmed as the main deformation mechanism of shear band initiation and propagation in metals under high strain rate loading. In fact, Park (2001) had pointed out the importance of dynamic recrystallization for modeling the stress collapse state inside dynamic ASBs.

The main idea of the current work is to select the DRX inside the ASB as the parallel process to model and use the modeling of the DRX inside the ASB as the feature characterization of the ASB propagation. The advantages of doing so are the following: (1) since DRX is the main feature accompanying the ASB propagation, they are dynamically synchronized, and they share many key characteristics, such as the onset as well as ending marks; (2) the conditions for the onset of DRX are relatively well established and are tied to the actual properties of the material.

It is well known that many factors affect the initiation of DRX in metals. Among them are the material's crystallographic structure, density of dislocations, initial grain size, and precipitates. However, the most important factors are the deformation conditions, such as strain rate and temperature. DRX occurs during deformation when temperature reaches some critical value (we denote it here as T_{DRX}), which may vary for different materials, but is usually between 0.4 and 0.5 of melting temperature. However, the value of T_{DRX} is also not constant for a given material. As follows from the experimental results, the value of the critical temperature is dependent on the strain rate and is lower for higher strain rates; this is clearly shown at the deformation mechanism maps given by Frost and Ashby (1982).

2.5. New criterion

Based on the above discussions, we propose a temperature-based ductile failure criterion for the ASB propagation. When temperature reaches the critical value, T_{cr}, which is a function of a strain rate, instant softening occurs, which leads to stress collapse. Since DRX does not occur for low values of strain rate, we suggest that T_{cr} is equal to the melting temperature, T_{m}, for low strain rates when no DRX takes place, and is equal to T_{DRX} for the higher strain rates. Combining the two cases in a single function which would provide a smooth transition between them, we derive T_{cr} in the following form:

$$T_{\mathrm{cr}} = T_{\mathrm{DRX}} + (T_{\mathrm{m}} - T_{\mathrm{DRX}}) \frac{\dot{\varepsilon}_{\mathrm{DRX}}}{\dot{\varepsilon}_{\mathrm{DRX}} + \dot{\varepsilon}}. \tag{4}$$

The above form was chosen also because it fits very well the shape of the DRX regions shown at the deformation mechanism maps that are based on the experimental observations (Frost and Ashby, 1982). Though the functional form of the new criterion is similar to that of the strain-based criterion (2), the parameters here have a completely different and well-defined physical meaning. Here T_{DRX} is a minimum temperature at which DRX is possible for this material at very high strain rates. Parameter $\dot{\varepsilon}_{\mathrm{DRX}}$ corresponds to the value of a strain rate at which the DRX begins to play an important role in the deformation mechanism. Around this value the transition of T_{cr} from T_{m} to T_{DRX} takes place. At $\dot{\varepsilon} = \dot{\varepsilon}_{\mathrm{DRX}}$ the critical temperature is equal to the median value $(T_{\mathrm{m}} + T_{\mathrm{DRX}})/2$ between the minimum recrystallization temperature and the melting temperature. When used in the numerical simulations along with a multi-physics constitutive model, the constitutive law at a material point can be switched to the new one that models the stress collapse state, when the temperature at that material point reaches the value $T = T_{\mathrm{cr}}$.

A graphic representation of the new criterion is given in Fig. 2. Here, the critical temperature is plotted as a function of strain rate and is represented by the thick blue line. For this plot, homologous temperature $T_{\mathrm{H}} = T/T_{\mathrm{m}}$ was used. The critical temperature reduces with the growth of strain rate, according to relationship (4). It asymptotically approaches T_{DRX} as the strain rate grows to infinity and is close to the melting temperature T_{m} when the strain rate is close to zero. The parameter values used here are: $T_{\mathrm{DRX}} = 0.4T_{\mathrm{m}}$ and $\dot{\varepsilon}_{\mathrm{DRX}} = 10^{0}$.

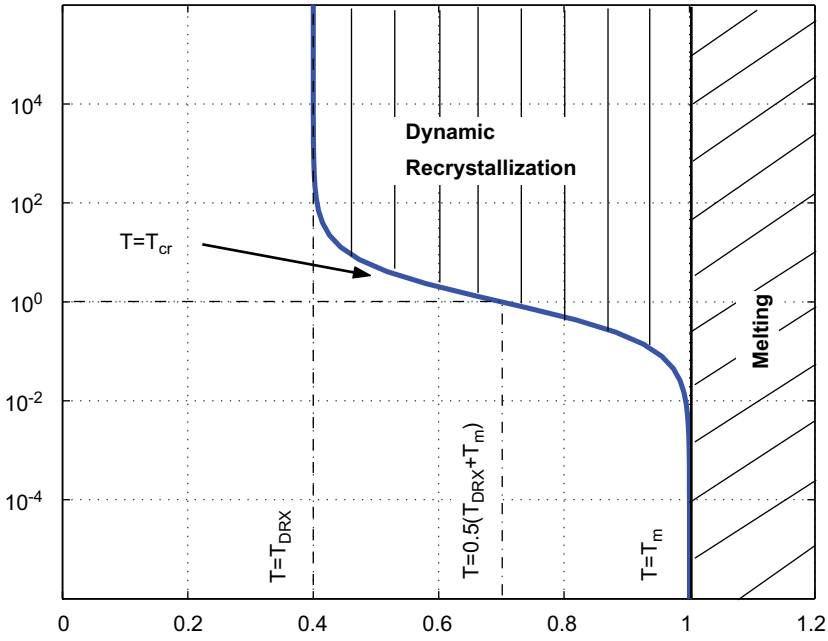

Fig. 2. Deformation mechanism map in the strain rate/temperature space. The curve representing the new failure criterion divides the space into two major parts: (1) undamaged area where regular thermo-elasto-viscoplastic constitutive law is applied and (2) the area where dynamic recrystallization or melting occurred and the stress collapse constitutive law has to be used.

A visual demonstration of the new criterion shown in Fig. 2 can be also viewed as a deformation mechanism map in a strain rate/temperature space. Here the whole space is divided into three parts: $T > T_m$ where melting of the material occurs, $T_{cr} < T < T_m$—area of DRX, and the rest of the domain. The new failure criterion allows for convenient separation of the first two areas (where the stress collapse has to be simulated) from the rest of the domain (where the initial thermo-elasto-viscoplastic constitutive law can be used) by a single curve representing the new failure criterion (4). The whole picture and the shape of the area of DRX are similar to the deformation mechanism maps given by Frost and Ashby (1982), which were generated based on the numerous experimental results.

It is important that the proposed new ductile failure criterion has a clear physical meaning, as it is based on DRX, a process that has been supported by a large number of experimental observations as a main deformation mechanism of shear banding at high strain rates. The parameters entering the new criterion, unlike those used in the previous criteria, are not free parameters; they are directly related to the material properties. The exact value for one of the parameters, melting temperature T_m, is readily available for most materials. Though exact measurements of the material parameters related to DRX, the recrystallization temperature T_{DRX} and the recrystallization strain rate $\dot{\varepsilon}_{DRX}$, are not known at this time, the approximate values are available from the experiments. Thus, as it was mentioned earlier, T_{DRX} is usually in the range of 0.4–0.5 of T_m, and, according to the deformation mechanism maps given by Frost and Ashby (1982), an appropriate value for $\dot{\varepsilon}_{DRX}$ is in the range of $10^{-4}-10^{0}$. In order to obtain more accurate values for these parameters, a thorough experimental work may be required. However, based on our observations, the given above approximate values are sufficient for meaningful predictions using the new criterion. Thus, reasonably close results were obtained for the ASB propagation using values of $\dot{\varepsilon}_{DRX}$ within the range of $10^{-4}-10^{0}$. This may be explained by the fact that ASB propagation is usually accompanied by very high strain rates (usually $\dot{\varepsilon} > 10^{2}$), which makes the dependency on $\dot{\varepsilon}_{DRX}$ somewhat weaker in this particular case. However, the general role of the parameter $\dot{\varepsilon}_{DRX}$ in the new criterion is very important. For instance, the parameter prevents the model from DRX and stress collapse at low values of strain rate, which would be completely non-physical.

In the following sections we test and validate the newly introduced criterion by applying it to numerical modeling of the initiation and propagation of dynamic ASBs.

3. Constitutive modeling

3.1. Thermo-viscoplastic material

We use an additive decomposition of the strain-rate tensor, $\mathbf{D}$, into elastic, viscoplastic, and thermal parts: $\mathbf{D} = \mathbf{D}^{elas} + \mathbf{D}^{vp} + \mathbf{D}^{ther}$. Stress rate is related to the elastic portion of the strain rate through the following constitutive equation:

$$\overset{\triangledown}{\boldsymbol{\tau}} = \mathbf{C}^{elas} : (\mathbf{D} - \mathbf{D}^{vp} - \mathbf{D}^{ther}), \tag{5}$$

where Jaumann rate of Kirchhoff stress, $\overset{\triangledown}{\boldsymbol{\tau}}$, is defined as

$$\overset{\triangledown}{\boldsymbol{\tau}} = \dot{\boldsymbol{\tau}} - \mathbf{W}\cdot\boldsymbol{\tau} + \boldsymbol{\tau}\cdot\mathbf{W}, \tag{6}$$

and $\mathbf{W}$ is a spin tensor. In (5) $\mathbf{C}^{\text{elas}}$ is the fourth order tensor of elastic moduli, and the thermal rate of deformation is given as $\mathbf{D}^{\text{ther}} = \alpha \dot{T}\mathbf{I}$, where α is the coefficient of thermal expansion and $\mathbf{I}$ is the second order identity tensor.

We employ constitutive relations of the J_2 flow theory of metal plasticity, see, e.g., Belytschko et al. (2000). The plastic flow rule is as follows:

$$\mathbf{D}^{\text{vp}} = \frac{3\dot{\bar{\varepsilon}}}{2\bar{\sigma}}\boldsymbol{\tau}^{\text{dev}}, \tag{7}$$

where

$$\boldsymbol{\tau}^{\text{dev}} = \boldsymbol{\tau} - \tfrac{1}{3}\text{tr}(\boldsymbol{\tau})\mathbf{I} \quad \text{is a deviatoric Kirchhoff stress,} \tag{8}$$

$$\bar{\sigma} = \sqrt{\tfrac{3}{2}\boldsymbol{\tau}^{\text{dev}} : \boldsymbol{\tau}^{\text{dev}}} \quad \text{is the von Mises effective stress,} \tag{9}$$

$$\bar{\varepsilon} = \int_0^t \dot{\bar{\varepsilon}}\,\mathrm{d}t \quad \text{is the accumulated effective plastic strain,} \tag{10}$$

and $\dot{\bar{\varepsilon}} = \sqrt{\frac{2}{3}\mathbf{D}^{\text{vp}} : \mathbf{D}^{\text{vp}}}$ is an effective plastic strain rate.

A Johnson–Cook material model is adopted (Johnson and Cook, 1985), which is described as

$$\dot{\bar{\varepsilon}} = \dot{\varepsilon}_0 \exp\left\{\frac{1}{C}\left(\frac{\bar{\sigma}}{g(\bar{\varepsilon}, T)} - 1\right)\right\}, \tag{11}$$

$$g(\bar{\varepsilon}, T) = [A + B\bar{\varepsilon}^n][1 - T^{*m}], \quad T^* = \frac{T - T_0}{T_{\text{m}} - T_0}, \tag{12}$$

where $\dot{\varepsilon}_0 = 1.0\,\text{s}^{-1}$ is a referential strain rate, n and m are correspondingly a strain hardening and a thermal softening exponents, T_0 is a reference (room) temperature, and T_{m} is a melting temperature.

The von Mises flow stress, $\bar{\sigma}$, can be expressed as

$$\bar{\sigma} = [A + B\bar{\varepsilon}^n][1 + C\ln(\dot{\bar{\varepsilon}}/\dot{\varepsilon}_0)][1 - T^{*m}], \tag{13}$$

and values of the parameters for the constitutive law given by Johnson and Cook (1985) are listed in Table 1.

For the constitutive update, we largely follow the rate tangent modulus method, which was proposed by Peirce et al. (1984) for rate-dependent solids and uses a linear interpolation within the time increment. For more detail on the application of this method readers may refer to Li et al. (2000, 2001, 2002).

Table 1
Johnson–Cook material model parameters

Parameter	4340 steel	OFHC copper
A (MPa)	792	90
B (MPa)	510	292
n	0.26	0.31
C	0.014	0.025
m	1.03	1.09

3.2. Damage model for the stress collapse state inside an ASB

The multi-physics approach adopts two types of constitutive relations to model an ASB: one inside the ASB, the other is the original constitutive relation of the ductile material. The constitutive relation inside the ASB is often referred to as "the damage model", which provides the post-localization stress collapse state inside an ASB.

A popular choice of modeling the stress collapse state inside an ASB is to use the so-called fluid model. For instance, Zhou et al. (1996b, 1998); Li et al. (2002) used

$$\boldsymbol{\tau} = -\frac{\gamma[1 - J + \alpha(T - T_0)]}{J}\frac{E}{1 - \nu}\mathbf{1} + \mu\mathbf{D}, \tag{14}$$

where $\boldsymbol{\tau}$ is a Kirchhoff stress tensor, γ is the stiffness parameter, μ is a viscosity coefficient, and $\mathbf{1}$ is an identity tensor.

Though, at the first sight, the use of a fluid model, in general, may be questionable, there is a growing amount of evidence that fluid-like material behaviors prevail inside an ASB. For instance, Guduru et al. (2001a,b) have reported experimental observations of vortical microstructures inside the ASBs, analogous to the classical instabilities in hydrodynamics. Previously, similar instabilities were found by Molinari and Leroy (1991), who studied the shear band formation in the earth's lower crust as well as in high strain rate torsional Kolsky bar tests (Leroy and Molinari, 1992). In their analysis, they used the following constitutive relation:

$$\boldsymbol{\sigma} = -p\mathbf{1} + 2\exp[-\beta(\theta - 1)]\dot{\gamma}^{m-1}\mathbf{D}, \tag{15}$$

which is essentially a non-Newtonian fluid, and where θ, p, $\dot{\gamma}$ are correspondingly the temperature, the pressure, and the effective strain rate. A similar viscous fluid constitutive law was used by Li et al. (2001) in their multi-physical modeling of ASB propagation:

$$\boldsymbol{\sigma} = -p\mathbf{1} + \mu^*(T)\mathbf{D} \quad \text{and} \quad \mu^*(T) = \mu_0 \exp\left[-\beta\left(\frac{T - T_0}{T_0}\right)\right], \tag{16}$$

where μ_0 and β are empirical constants.

The DRX-based mechanism of deformation inside an ASB presented in Section 2 also provides a further justification for using viscous fluid as a constitutive model for simulating a stress collapse state inside the ASBs. During DRX, the material behavior inside an ASB is quite similar to that of a viscous fluid, so that some authors even used the term "fluidity" for its description (Mescheryakov and Atroshenko, 1995). A viscous fluid constitutive law would be suitable for modeling deformation processes that occur by some kind of grain-boundary sliding mechanisms. Now it is widely accepted that such mechanisms play an important role during high-strain rate deformation inside ASBs (Murr et al., 2002). Additionally, it is believed that very large plastic deformations, so-called superplasticity, occur by sliding of the micrograin boundaries (see, e.g., Cahn and Haasen, 1996). Furthermore, the proposed mechanisms of DRX inside ASBs (Meyers and Pak, 1986; Hines and Vecchio, 1997) involve sliding of elongated grains at the first stages of DRX, as well as rotation and sliding of the equiaxed grains at the final stages of the DRX process.

4. Numerical simulation results

In our simulations, we employ one of the so-called meshless, or mesh-free, methods (see, e.g., Belytschko et al., 1994). The particular meshless method used in this work is the reproducing kernel particle method (RKPM) (Liu et al., 1995a,b, 1997). A comprehensive review of meshless methods and their applications can be found in the article by Li and Liu (2002) and in the book recently published by the same authors (Li and Liu, 2004). Employing Galerkin weak formulations for both linear momentum and energy equations, we solve a coupled thermo-mechanical problem. Details regarding the numerical implementation may be found in Zhou et al. (1996b); Li et al. (2001, 2002).

4.1. Problem statement

Numerical simulations were carried out using the following benchmark problem. A rectangular specimen 4×5 mm (see Fig. 3) is subject to a shear loading. The top side of the specimen is rigidly fixed and the bottom side is moved in the horizontal direction with a constant velocity v_L ($v_L = 30$ m/s if not mentioned otherwise). At the left side, there is a notch in the middle of the specimen, 1 mm long and 260 μm wide, and a small precrack (260 μm long) extends from the tip of the notch in the $y = 2$ mm plane (the precrack is not visible in the figure). A defect, such as the precrack, is necessary to create an imperfection, which serves as a stress concentrator and is needed in order for a shear band to initiate.

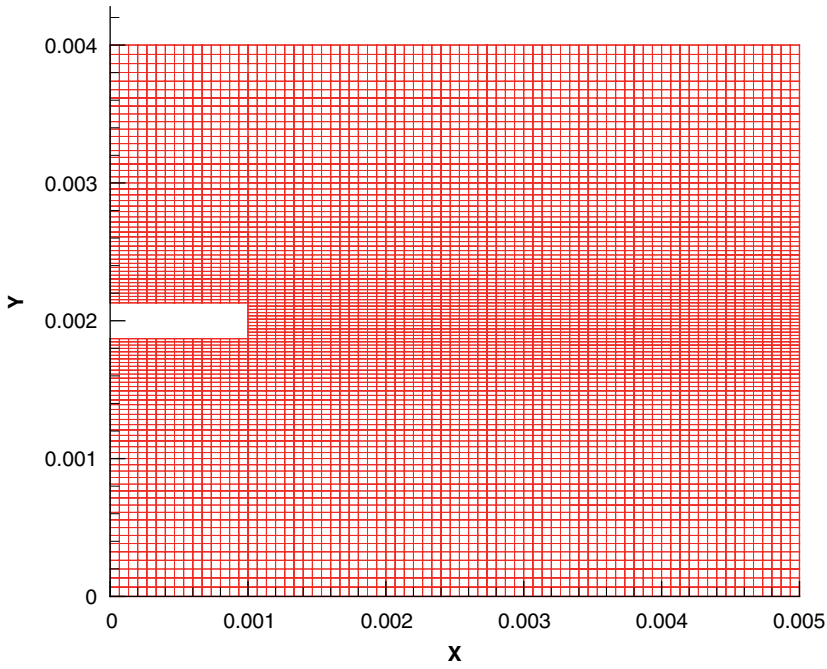

Fig. 3. Initial undeformed configuration. Shown background mesh was used to create a grid of particles. Dimensions are given in meters.

Three different grids of particles were used in these simulations. The background mesh for the coarsest grid is shown in Fig. 3. Each node of this mesh represents a particle used in the meshless interpolation. The smallest distance between the particles in this grid is approximately 24 μm and is applied in the refined area in the middle of the specimen with total eleven background mesh cells across the notch width. We will refer to this grid as a "coarse" grid. The two other grids are approximately two and four times finer and will be called "medium" and "fine" correspondingly. The smallest inter-particle distances for those grids are approximately 12 and 6 μm. Most of the results presented here were obtained using the coarse and medium grids, while the fine grid (the most computationally expensive) was only used to study the mesh-dependency of the obtained solutions.

In our simulations we use two materials, 4340 steel and OFHC copper. The values of the material parameters are listed in Table 2. Adiabatic shear banding has been observed experimentally in these materials (see, e.g., Bai and Dodd, 1992), even though the occurrence of the adiabatic shear localization in copper is more rare than in steel. The main reason for choosing these two materials for our studies was that they have very different thermal properties and shear band characteristics. The heat conductivity of OFHC copper is 10 times larger than that of the 4340 steel, and the effect of heat conduction, which we have investigated in our simulations, is much larger for copper. In addition, the shear band width in copper is much larger than that in steel, while the general susceptibility to a failure via shear banding is higher for steel.

4.2. Simulations without damage model

Before we present results of our simulations using the damage model explained in Section 3.2 and the ductile failure criterion introduced in Section 2.5, we want to show what happens if no damage model, and therefore no failure criterion, is used at all to model the stress collapse state inside an ASB. This step is needed to justify the necessity of damage model and failure criterion for modeling the ASB propagation.

Fig. 4 shows temperature and effective stress contours of the deformed copper specimen at two different moments of time: 40 and 60 μs. At first, the shear band seems to initiate and propagate to some extent, but than it gets arrested and never propagates through the whole specimen even if the shear loading continues for a long time and at a considerable

Table 2
Material parameters used in the simulations

Parameter	Definition	4340 steel	OFHC copper
E	Young's modulus (GPa)	200	124
ν	Poisson's ratio	0.29	0.34
ρ	Mass density (kg/m^3)	7830	8960
k	Heat conductivity (W/mK)	38	386
C_p	Specific heat (J/kgK)	477	383
α	Coeff. of thermal expansion (K^{-1})	32×10^{-6}	50×10^{-6}
T_m	Melting temperature (K)	1793	1356
T_{DRX}	Recrystallization temperature ($0.4\,T_m$)	717.2	542.4
T_0	Reference (room) temperature (K)	293	293
χ	Fract. of plastic work converted to heat	0.9	0.9
μ	Damage model viscosity (Pa s)	500	500

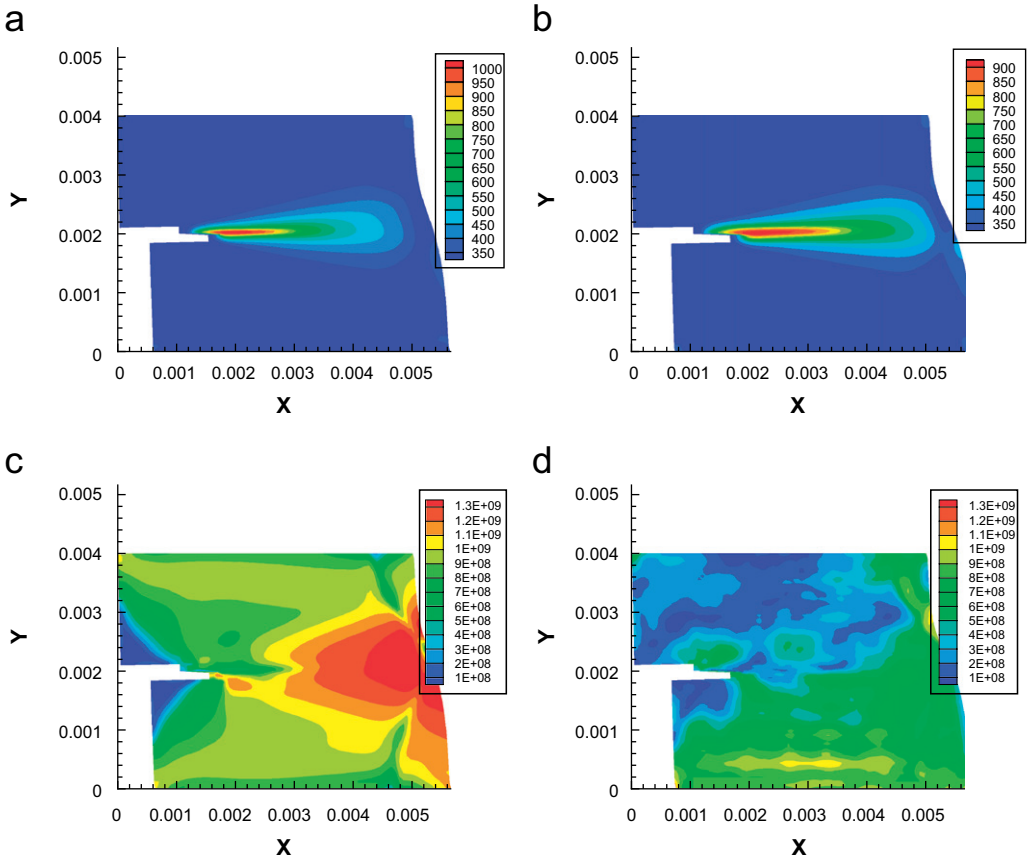

Fig. 4. Simulations without damage model. Temperature and effective stress contours. Shear band gets arrested and does not propagate through the specimen. (a) temparature, 40 μs (b) temparature, 60 μs (c) effective stress, 40 μs (d) effective stress, 60 μs.

velocity of 30 m/s. The stress contour plots show that even if the stress values are quite high at 40 μs, there is no high stress concentration just in front of the shear band tip, and stresses are considerably lower at 60 μs, showing rather homogeneous than localized plastic deformation between the arrested band tip and the end of the specimen.

It seems that this diffuse nature of stress and deformation around the anticipated shear band tip area is the main reason for its arrest. We believe this is caused by too high resistance of the material *inside* the already formed band, which was modeled by the same constitutive law as the rest of the specimen.

4.3. Simulations with damage model

4.3.1. General observations

Now we present results of simulations when damage model of Section 3.2 was used along with the newly introduced ductile failure criterion of Section 2.5. The shear band propagation was successfully modeled for both types of materials, copper and steel. Upon

applied loading, stress, strain, and temperature concentrate around the precrack, and after some time the shear band initiates from the tip of the crack and propagates in a horizontal direction through the whole specimen.

The total duration of the modeled deformation process is 40 μs. Fig. 5 shows the temperature contours for copper specimen at four moments of time: $t = 10$, 20, 30 and 40 μs. Based on our observations, the whole process of the shear band initiation and propagation here can be divided into four main stages: (1) build-up of plastic deformation and heat in the crack tip area, initial localization of deformation; (2) shear band initiation and propagation through the specimen; (3) after shear band reaches the end of the specimen, it continues to grow in width due to heat conduction through the sides of the band; (4) the shear band width stabilizes at some finite value while relative sliding of the two parts of the specimen continues.

Typical effective stress contours during the shear band initiation and propagation are shown in Fig. 6. Here, the results of the simulations using multi-physics approach, i.e., with damage model, and those not using any damage model are collated. The right plot

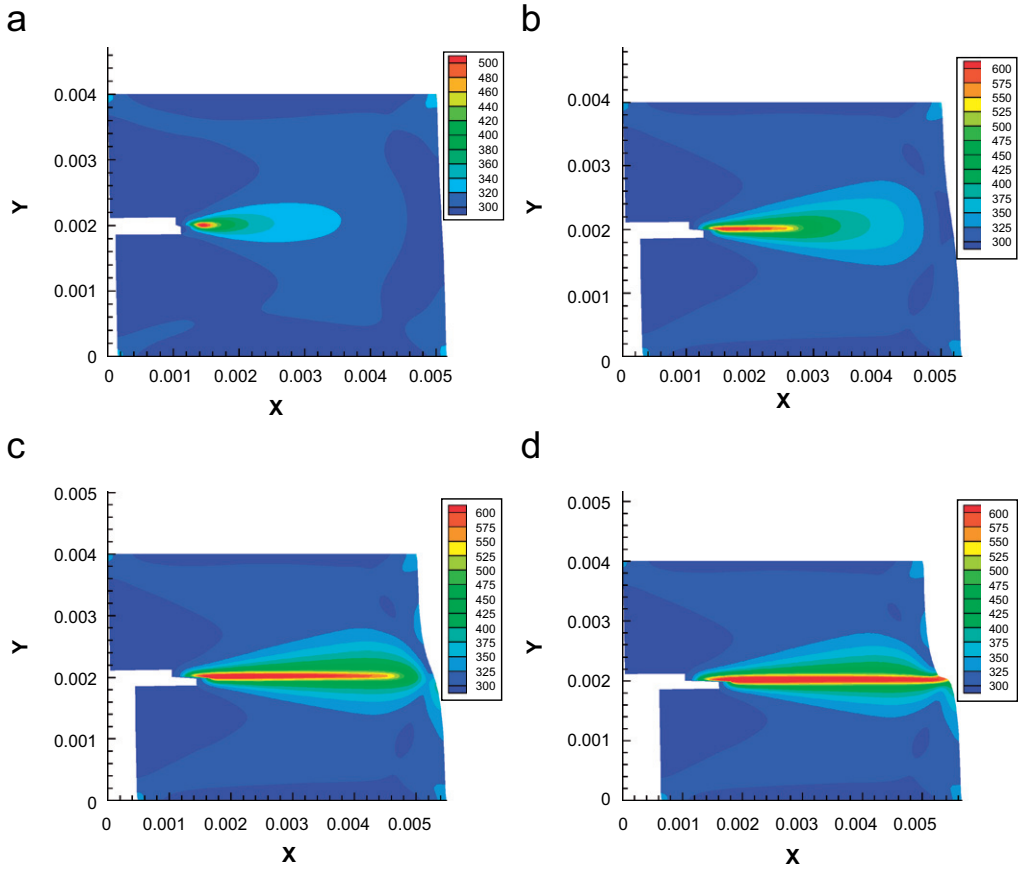

Fig. 5. Shear band initiation and propagation. Copper specimen. Temperature contours (K). (a) time = 10 μs (b) time = 20 μs (c) time = 30 μs (d) time = 40 μs.

(with damage model) shows the shear band propagating through the specimen and corresponds to the temperature plot of Fig. 5(b), $t = 20\,\mu s$; while the left plot (without damage model), same as Fig. 4(c), shows the shear band being arrested in the middle of the specimen. One big difference can be noticed when comparing the two plots. There is a high gradient of stress just in front of the shear band tip in the right plot, whereas the stress field is rather diffuse and there is no concentration in front of the tip in the left plot, when a single constitutive law was used to model the whole specimen.

4.3.2. *Shear band length, time of initiation, and speed of propagation*

Shear band length histories at different loading velocities, $v_L = 20, 25, 30, 35\,m/s$, for both steel and copper are given in Fig. 7. These plots provide information about the time of the shear band initiation, when the band reaches the end of the specimen, as well as the speed of propagation.

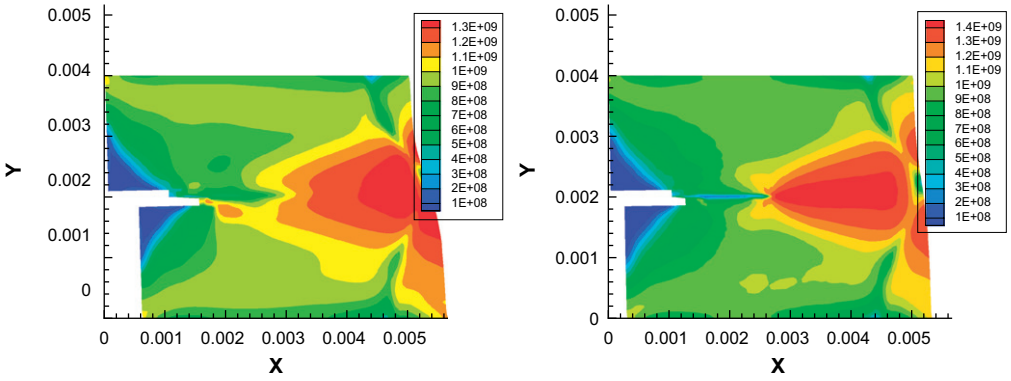

Fig. 6. Effective stress contours during shear band propagation, without damage model (left, $t = 40\,\mu s$) and with damage model (right, $t = 20\,\mu s$).

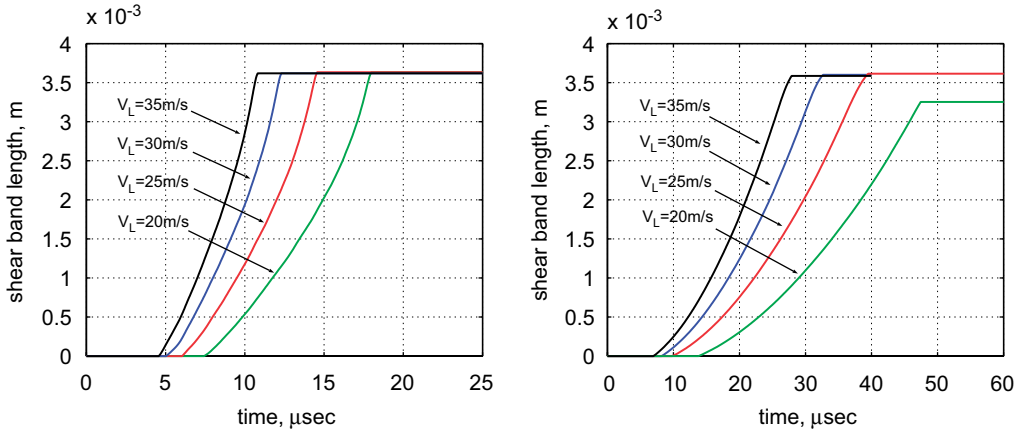

Fig. 7. Shear band length histories at different loading velocities, v_L, for steel (left) and copper (right) specimens.

The shear band length histories are quite different for the two types of material. The ASB starts earlier and propagates much faster in the steel specimen than in the copper one. For instance, at the loading velocity of 30 m/s (shown blue in the figure) in case of the steel specimen, shear band initiated approximately at $t = 5\,\mu s$ and reached the end of the specimen at about $t = 12.3\,\mu s$. At the same loading velocity, for the copper specimen shear band initiated at about $t = 8.2\,\mu s$ and reached the end of the specimen at $t = 32.6\,\mu s$. Note that the shear band initiated much earlier in case of steel, even though the required critical temperature was higher for steel ($T_{cr} \approx 717.2\,K$) than for copper ($T_{cr} \approx 542.4\,K$). This observation shows the crucial role of heat conduction in the process of shear band initiation. Because heat conductivity of copper is approximately 10 times that of steel, it took much longer for copper to reach the lower critical temperature value. The total time that took the shear band to propagate through the whole specimen was 7.3 μs for steel and 24.4 μs for copper. In addition, in the case of copper the shearband did not propagate through the whole specimen when the loading velocity was too low, 20 m/s, whereas in case of steel the shear band propagated till the end of the specimen for all the investigated loading velocities.

Shear band speed histories at different loading velocities, v_L, for both types of materials are shown in Fig. 8. The overall shapes of the history curves are also different for the two materials. While for copper the shear band grows steadily and then after reaching a peak goes down near the end of the specimen, in the case of steel the speed grows steadily until the band tip reaches approximately the middle of the specimen and after that the grow increases, reaches the high peak and then drops.

Fig. 9 shows the average and maximum shear band speeds for both materials at different loading velocities. We can see that the average speed of shear band propagation is approximately three times larger for steel than for copper. With the loading velocity increasing, the maximum speed goes up for both types of material. However, while for copper it seems to grow nearly linearly, in case of steel the maximum speed seems to slow down its grow and reach a plateau after $v_L = 30\,m/s$. The maximum shear band speeds were 1174 m/s for steel and 300 m/s for copper and were observed at $v_L = 40\,m/s$.

Values obtained for steel can be compared to the experimental results by Zhou et al. (1996a) and Guduru et al. (2001a), as well as simulation results by Li et al. (2002). Though

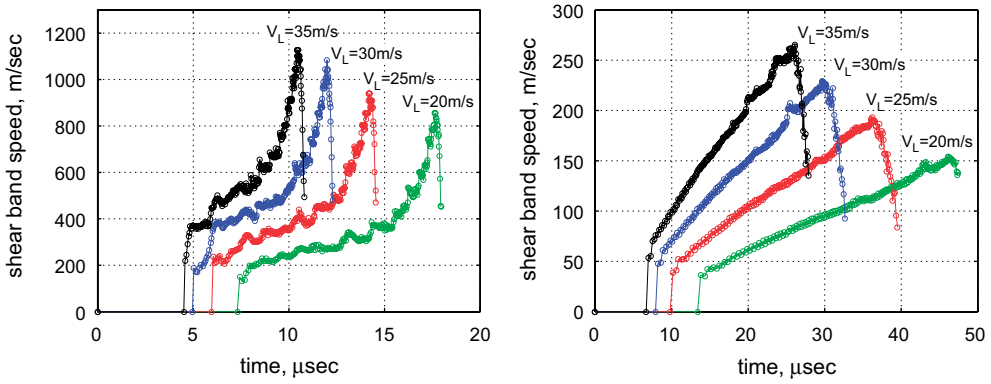

Fig. 8. Shear band speed histories at different loading velocities, v_L, for steel (left) and copper (right) specimens.

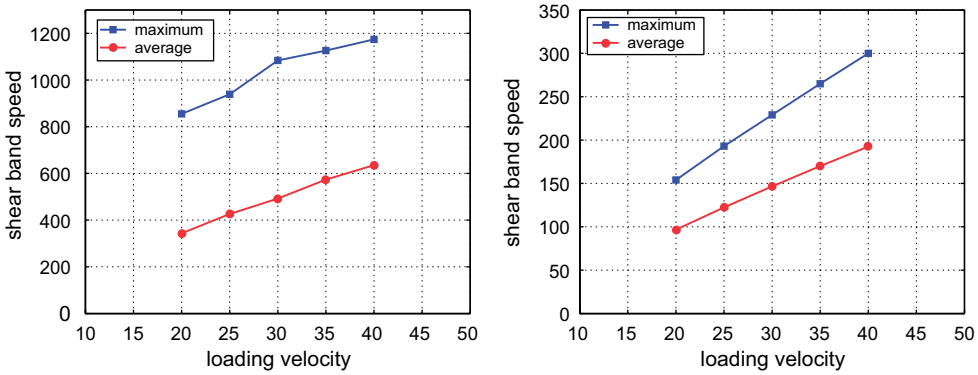

Fig. 9. Average and maximum shear band speeds vs. loading velocity for steel (left) and copper (right) specimens.

Table 3
Summary of the current simulation results

		Current simulations	Experimental observations
Maximum speed	Steel	1174	~1200[a], ~1100[b]
(m/s)	Copper	300	–
Max. temperature	Steel	~1100	~1150[a], >900[b]
(K)	Copper	~650	–
Shear band width	Steel	~50	~40[b]
(μm)	Copper	~120	100–300[c]

[a]Comparison to experimental observations: Zhou et al. (1996a).
[b]Comparison to experimental observations: Guduru et al. (2001a).
[c]Comparison to experimental observations: common observations.

they used C300 steel, we believe that the comparison may be appropriate since the material properties of the two types of steel are reasonably close. The maximum shear band speed in the experiments by Zhou et al. (1996a) was close to 1200 m/s and was observed at the loading velocity of 30 m/s. Guduru et al. (2001a) reported the maximum shear band speed of about 1100 m/s which was observed at the loading velocity of 36 m/s. These results are summarized in Table 3. Simulations by Li et al. (2002), who used a different type of ductile failure criterion, gave much higher values for the shear band speed, up to 2000 m/s. In those simulations they used the strain-based criterion (2) described in Section 2.2.

4.3.3. Shear band width and mesh independency

Probably the most important differences between the current simulation results and those of the previous simulations are related to the width of the obtained shear bands. Due to the heat conduction implemented in the model and the new ductile failure criterion introduced in Section 2, the shear band width is resolved and now spans across several background mesh cells, as shown in Figs. 10 and 11. These pictures of ASBs look more natural and physically sound than the ones obtained from previous calculations that used older versions of the ductile failure criterion (e.g., compare to Fig. 1).

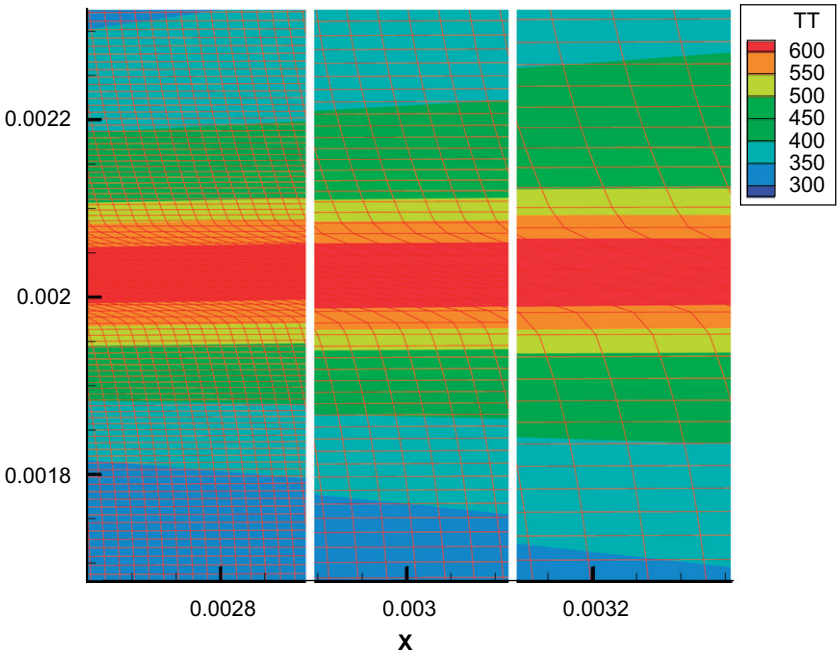

Fig. 10. A fully developed shear band modeled using new failure criterion. Temperature contours (K). Copper specimen. Three grids have different particle densities: fine (left), medium (center) and coarse (right).

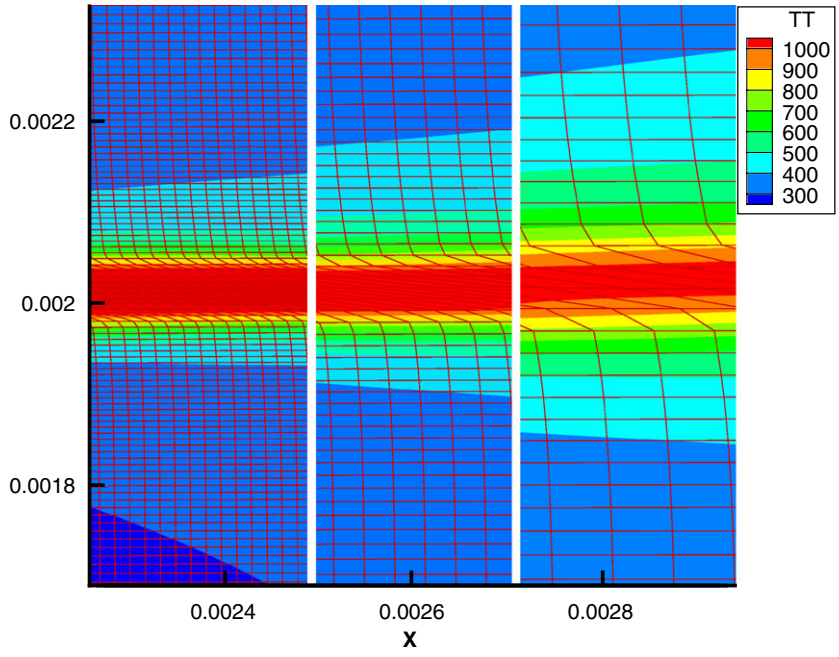

Fig. 11. A fully developed shear band modeled using new failure criterion. Temperature contours (K). Steel specimen. Three grids have different particle densities: fine (left), medium (center), and coarse (right).

Figs. 10 and 11 show the temperature profiles and deformed background meshes of the shear band regions for copper and steel specimens correspondingly. These pictures demonstrate that the results are now quite mesh independent. They show the resolved shear band width obtained using three different grids of particles: fine, medium, and coarse. The comparison reveals a very close agreement, both qualitative and quantitative, between the three simulations for each material. A good qualitative agreement here can be seen in a general deformation pattern of the shown background meshes, which can be viewed as the material (Lagrangian) coordinate lines that are frozen in the material. The deformation patterns are almost identical for all the three different types of meshes. In addition, a good quantitative agreement between the three simulation results for each type of material can be seen in the temperature contours as the same scale was used for all the three contour plots.

The observed shear band width here is on the order of 120 μm for copper and 50 μm for steel, though it is difficult to exactly define the width because of the gradual onset of the localization of deformation across the shear band's boundaries (especially in the case of copper). Nevertheless, the obtained values are quite close to the experimentally observed shear band widths, which are usually reported to be between 100 and 300 μm for copper and between 30 and 60 μm for steel. Thus, for steel Guduru et al. (2001a) observed the shear band width of about 40 μm. We believe that in our simulations we observe the lower bound of the predicted value for copper because the shear band width may not have completely stabilized by $t = 40\,\mu s$, and the shear band still continues to grow in width due to the heat conduction from the shear band core into the surrounding areas.

In addition, we can compare the observed temperature rises to the known experimental results for steel. The maximum temperature inside an ASB at the loading velocity of 30 m/s has almost reached 1100 K. Very similar results were reported by experimentalists. For the loading velocity of 33 m/s, Zhou et al. (1996a) have measured the maximum temperature of approximately 1150 K. Guduru et al. (2001a) reported a temperature of approximately 900 K, but noted that due to the particular experimental technique employed, the experimental value underestimates the actual temperature inside the ASB. The simulation results are summarized and compared to experimental observations in Table 3.

In general, we may conclude that the values obtained in the current simulations for important ASB quantities, such as speed of propagation, shear band widths, and temperature increases, are very close to those observed in the experiments. This gives further credibility to the applied modeling techniques and, in particular, the newly proposed ductile failure criterion.

5. Conclusions

In this work, a new ductile failure criterion was proposed based on the DRX deformation mechanism. The new criterion was formulated in terms of temperature and strain rate and can be used to predict the onset of ductile failure as well as for modeling the initiation and propagation of dynamic ASBs. The main advantage of the current criterion is its clear physical basis, and, as a result, clear physical meaning of its parameters, such as melting and recrystallization temperatures, that are readily available for most materials. In addition, the relative simplicity of the proposed criterion makes it very easy to implement in numerical simulations. Large scale parallel computations have been carried out to test and verify the newly proposed criterion used along with the multi-physics constitutive

modeling. The results of the numerical simulations were found to be in close agreement with experimental observations regarding various characteristic features of dynamic ASBs, such as the shear band width, speed of propagation, and temperature rise inside an ASB. Moreover, we have examined the effects of heat conduction on the formation and propagation of ASBs. Specifically, we have studied the relationship between the effect of heat conduction, the shearband width, and the numerical mesh-dependency or mesh-sensitivity. It is shown that moderate and strong heat conduction used along with the proposed ductile failure criterion stabilize the lateral spatial dimension of the ASB, and as a result, a physically meaningful numerical solution can be attained. Finally, the fact that the proposed ductile failure criterion allows for the realistic modeling of the ASB initiation and propagation serves as an additional support to the assumption of DRX occurring inside the ASBs.

Acknowledgments

The authors gratefully acknowledge support from the National Science Foundation and Army Research Office. S.L. would like to acknowledge the support from the National Science Foundation through Grant no. CMS-0239130 to the University of California.

References

Andrade, U., Meyers, M.A., Vecchio, K.S., Chokshi, A.H., 1994. Dynamic recrystallization in high-strain, high-strain rate plastic deformation of copper. Acta Metall. Mater. 42, 3183–3195.

Areias, P.M.A., Belytschko, T., 2006. Two-scale shear band evolution by local partition of unity. Int. J. Numer. Meth. Eng. 66, 878–910.

Bai, Y.L., Dodd, B., 1992. Adiabatic Shear Localization. Pergamon Press, Oxford.

Batra, R.C., Kim, C.H., 1992. Analysis of shear banding in twelve materials. Int. J. Plasticity 8, 425–452.

Batra, R.C., Lear, M.H., 2004. Simulation of brittle and ductile fracture in an impact loaded prenotched plate. Int. J. Fract. 126 (2), 179.

Belytschko, T., Lu, Y.Y., Gu, L., 1994. Element-free Galerkin methods. Int. J. Numer. Meth. Eng. 37 (2), 229–256.

Belytschko, T., Liu, W.K., Moran, B., 2000. Nonlinear Finite Elements for Continua and Structures. Wiley, New York.

Bonnet-Lebouvier, A.-S., Molinari, A., Lipinski, P., 2002. Analysis of the dynamic propagation of adiabatic shear bands. Int. J. Solids Struct. 39 (16), 4249–4269.

Cahn, R.W., Haasen, P., 1996. Physical Metallurgy, vol. 3. North-Holland, Amsterdam.

Frost, H.J., Ashby, M.F., 1982. Deformation-mechanism Maps: the Plasticity and Creep of Metals and Ceramics. Pergamon Press, New York.

Guduru, P.R., Rosakis, A.J., Ravichandran, G., 2001a. Dynamic shear bands: an investigation using high speed optical and infrared diagnostics. Mech. Mater. 33, 371–402.

Guduru, P.R., Ravichandran, G., Rosakis, A.J., 2001b. Observations of transient high temperature vortical microstructures in solids during adiabatic shear banding. Phys. Rev. E 64, 036128-1-6.

Hines, J.A., Vecchio, K.S., 1997. Recrystallization kinetics within adiabatic shear bands. Acta Mater. 45 (2), 635.

Hines, J.A., Vecchio, K.S., Ahzi, S., 1998. Model for microstructure evolution in adiabatic shear bands. Metall. Mater. Trans. A 29A, 191.

Johnson, G.R., Cook, W.H., 1985. Fracture characteristics of three metals subjected to various strains, strain rates, temperatures and pressures. Eng. Fract. Mech. 21 (1), 31–48.

Leroy, Y.M., Molinari, A., 1992. Stability of steady states in shear zones. J. Mech. Phys. Solids 40, 181–212.

Li, S., Liu, W.K., 2002. Meshfree and particle methods and their applications. Appl. Mech. Rev. 55, 1–34.

Li, S., Liu, W.K., 2004. Meshfree Particle Methods. Springer, Berlin, 502pp.

Li, S., Hao, W., Liu, W.K., 2000. Mesh-free simulations of shear banding in large deformation. Int. J. Solids Struct. 37 (48–50), 7185–7206.

Li, S., Liu, W.K., Qian, D., Guduru, P.R., Rosakis, A.J., 2001. Dynamic shear band propagation and microstructure of adiabatic shear band. Comput. Methods Appl. Mech. Eng. 191 (1–2), 73–92.

Li, S., Liu, W.K., Rosakis, A.J., Belytschko, T., Hao, W., 2002. Mesh-free Galerkin simulations of dynamic shear band propagation and failure mode transition. Int. J. Solids Struct. 39 (5), 1213–1240.

Liu, W.K., Jun, S., Li, S., Adee, J., Belytschko, T., 1995a. Reproducing kernel particle methods for structural dynamics. Int. J. Numer. Meth. Eng. 38, 1655–1679.

Liu, W.K., Jun, S., Zhang, Y., 1995b. Reproducing kernel particle methods. Int. J. Numer. Meth. Fluids 20 (8–9), 1081–1106.

Liu, W.K., Li, S., Belytschko, T., 1997. Moving least square reproducing kernel method part i: methodology and convergence. Comput. Methods Appl. Mech. Eng. 143, 422–433.

Marchand, A., Duffy, J., 1988. An experimental study of the formation process of adiabatic shear bands in a structural steel. J. Mech. Phys. Solids 36 (3), 251–283.

McQueen, H.J., Bergerson, S., 1972. Dynamic recrystallization of copper during hot torsion. Met. Sci. J. 6, 25–29.

Mescheryakov, Yu.I., Atroshenko, S.A., 1995. Dynamic recrystallization in shear bands. In: Murr, L.E., Staudhammer, K.P., Meyers, M.A. (Eds.), Metallurgical and Materials Application of Shock-Wave and High-Strain-Rate Phenomena. Elsevier Science B.V., Amsterdam, pp. 443–450.

Meyers, M.A., 1994. Dynamic Behavior of Materials. Wiley, New York.

Meyers, M.A., Pak, H.R., 1986. Observation of an adiabatic shear band in titanium by high voltage transmission electron microscopy. Acta Met. 34, 2493–2499.

Meyers, M.A., Nesterenko, V.F., LaSalvia, J.C., Xue, Q., 2001. Shear localization in dynamic deformation of materials: microstructural evolution and self-organization. Mat. Sci. Eng. A 17, 204–225.

Molinari, A., Leroy, Y.M., 1991. Structures in shear zones due to thermal effects. C.R. Acad. Sci. Paris, Ser. II 313, 7–13.

Murr, L.E., Trillo, E.A., Pappu, S., Kennedy, C., 2002. Adiabatic shear bands and examples of their role in severe plastic deformation. J. Mater. Sci. 37, 3337–3360.

Nesterenko, V.F., Meyers, M.A., LaSalvia, J.C., Bondar, M.P., Chen, Y.J., Lukyanov, Y.L., 1997. Investigation of high-strain, high-strain rate behavior of tantalum using the collapse of a thick-walled cylinder. Mat. Sci. Eng. A 229, 23–41.

Park, H.S., 2001. Meshfree simulations of dynamic adiabatic shearbands. Master's Thesis.

Peirce, D., Shih, C.F., Needleman, A., 1984. A tangent modulus method for rate dependent solids. Comput. Struct. 18 (5), 875–887.

Schoenfeld, S.E., Wright, T.W., 2003. A failure criterion based on material instability. Int. J. Solids Struct. 40, 3021–3037.

Wright, T.W., 1990. Approximate analysis for the formation of adiabatic shear bands. J. Mech. Phys. Solids 38, 515–530.

Wright, T.W., 2002. The Physics and Mathematics of Adiabatic Shear Bands. Cambridge University Press, Cambridge.

Xu, Y.B., Zhong, W.L., Chen, Y.J., Shen, L.T., Liu, Q., Bai, Y.L., Meyers, M.A., 2001. Shear localization and recrystallization in dynamic deformation of 8090 Al–Li alloy. Mat. Sci. Eng. A 299, 287–295.

Zhang, Z., Clifton, R.J., 2003. Shear band propagation from a crack tip. J. Mech. Phys. Solids 51 (11–12), 1903–1922.

Zhou, M., Rosakis, A.J., Ravichandran, G., 1996a. Dynamically propagating shear bands in impact-loaded prenotched plates—1. Experimental investigations of temperature signatures and propagation speed. J. Mech. Phys. Solids 44 (6), 981–1006.

Zhou, M., Ravichandran, G., Rosakis, A.J., 1996b. Dynamically propagating shear bands in impact-loaded prenotched plates—2. Numerical simulations. J. Mech. Phys. Solids 44 (6), 1007–1032.

Zhou, M., Rosakis, A.J., Ravichandran, G., 1998. On the growth of shear bands and failure-mode transition in prenotched plates: a comparison of singly and doubly notched specimens. Int. J. Plasticity 14 (4–5), 435–451.